Jordanian Journal of Computers and Information Technology (JJCIT), Vol. 2, No. 1, April 2016.

A COMPACT PRINTED UWB PACMAN-SHAPED MIMO ANTENNA WITH TWO FREQUENCY REJECTION BANDS

Shaimaa Naser[1] and Nihad Dib[2]

Department of Electrical Engineering, Jordan University of Science and Technology
P. O. Box 3030, Irbid 22110, Jordan.
[2]At the present time, on sabbatical leave at German Jordanian Univ.
naser.shaimaa@yahoo.com[1], nihad@just.edu.jo[2]

(Received: 23-Nov.-2015, Revised: 13-Dec.-2015, Accepted: 07-Jan.-2016)

ABSTRACT

In this paper, the design, analysis and prototyping of a microstrip-fed, low profile, compact ultra-wideband (UWB) monopole antenna with two band notches are presented. The antenna is then used in two multiple-input multiple-output (MIMO) configurations. The antennas are mounted on a low cost FR-4 substrate of a dielectric constant of 4.4. The original shape of the single antenna element is circular with a radius of 11.5 mm, then a sector is removed from the patch (making it a Pacman-shaped antenna) to improve the impedance bandwidth. The proposed antennas provide an impedance bandwidth between 2.9-15 GHz with better than 10 dB return loss and isolation of more than 16 dB and 19 dB for the first and the second MIMO configurations, respectively. Additionally, the antennas can reject the interferences from Worldwide Interoperability for Microwave Access (WiMAX) (3.5 GHz center frequency) and Wireless Local Area Network (WLAN) (5.5 GHz center frequency).

KEYWORDS

Ultra-wideband (UWB) antennas, Circular monopole antenna, Multiple-Input Multiple-Output (MIMO).

1. INTRODUCTION

Modern mobile systems require high speed and reliable transmission of data without an increment in bandwidth or transmitted power. Multiple-input multiple-output (MIMO) communication is the way to achieve the aforementioned goals through using multiple antennas, which are suitable for modern standard communications, such as WiFi, WiMAX, 4G, High Speed Packet Access (HSPA+) and UWB. MIMO is based on the use of multiple transmitting and receiving antennas to achieve spatial diversity or spatial multiplexing. Nowadays, UWB MIMO antennas are widely used due to the advantages of providing reliable and high data rate transmission.

Many studies have been conducted on the design and analysis of UWB MIMO antennas. In [1], a planar monopole UWB MIMO antenna that consists of two identical monopoles and a Y-shaped decoupling network fixed on the ground plane was investigated. The Y-shaped decoupling network provides an isolation of more than 20 dB and a correlation of less than 0.01. In [2], a compact UWB MIMO antenna with better than 15 dB isolation was proposed. The antenna elements were circular disc monopole antennas with a common ground. The isolation was improved through using an inverted-Y stub inserted on the ground. MIMO antennas can be designed to have two polarizations to achieve diversity. In [3], a single radiator was shared between two antenna elements, while diversity was achieved through having two different

polarizations. A stub in the ground and a T-shaped slot were etched from the radiator to enhance isolation. In [4], a dual polarization MIMO antenna was proposed through using two monopole antenna elements perpendicular to each other. Rejection of the WLAN band was achieved through etching an H-shaped slot and a resonant L-shaped strip.

In [5], two identical antenna elements were used to form an UWB MIMO antenna with 17 dB isolation. The single element consisted of seven circles surrounding a central circle. In [6], a UWB diversity slot antenna was investigated. The structure of the antenna consisted of two modified coplanar waveguides (CPWs) feeding staircase-shaped radiating elements for orthogonal radiation patterns, where a rectangular stub was placed between the two feeding CPWs to ensure high isolations. By etching two split-ring resonator (SRR) slots on the radiators, the band-notched property was achieved. In [7], an ultra-wideband MIMO antenna, which consisted of two elliptical-shaped monopoles, was proposed. Two stubs and a slot were introduced to reduce the mutual coupling between the two elements. Results showed that the antenna works in the band 3.1-10.6 GHz and has an isolation of more than 20 dB. In [8], a compact MIMO antenna that covers the WLAN (2.4 GHz) and UWB range was presented. The proposed antenna consisted of two open L-shaped slot antenna elements and a narrow slot on the ground plane. The isolation was larger than 20 dB in the WLAN band and 18 dB in the UWB range. Finally, [9] proposed a MIMO antenna in which each element consisted of a planar-monopole antenna printed on one side of the substrate, where the elements were placed perpendicular to each other. To enhance isolation and increase impedance bandwidth, two long protruding ground stubs were added to the ground plane. The antenna achieved an isolation larger than 15 dB and a correlation of less than 0.2 in the UWB range.

2. SINGLE UWB ANTENNA

Figure 1 illustrates the structure of the single UWB antenna. The antenna is mounted on a compact size FR-4 substrate of dimensions 25 × 38 mm^2, a dielectric constant of 4.4, a loss tangent of 0.02 and a thickness of 1.6 mm. The original patch has a circular shape, since it has the largest bandwidth among the other regular shapes and has good radiation characteristics [10]. The radius was approximated to be λ/4 at the lower frequency edge of the UWB range [11]. A partial ground plane is used with a notch cut near the feeding line to improve the impedance bandwidth. It has been found that the distance between the feeding point and the ground plane ($p = L_{feeding} - W_{gnd}$) has an effect on the antenna performance. Its value was chosen to be 0.2 mm. Then, a sector was removed from the circular patch (making it a *Pacman*-shaped antenna) to improve the impedance bandwidth. Finally, a U-shaped slot and a straight slot were etched in the patch to reject the interference from WiMAX and WLAN [12], respectively. The total lengths of the slots were approximated to be λ/2 at the notched frequencies [13]-[15]. Several simulations were performed using HFSS version 14 [16] to get the optimized parameters listed in Table 1. The simulated and the measured VSWR of the proposed UWB antenna are illustrated in Figure 2.

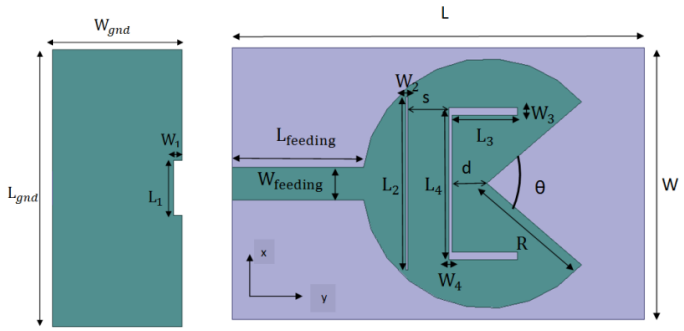

Figure 1. The structure of the proposed UWB antenna.

Jordanian Journal of Computers and Information Technology (JJCIT), Vol. 2, No. 1, April 2016.

Table 1. The optimized parameters of the proposed UWB antenna.

Parameter	Value	Parameter	Value
L	38 mm	W	25 mm
$L_{feeding}$	12 mm	$W_{feeding}$	3 mm
L_{gnd}	25 mm	W_{gnd}	11.8 mm
R	11.5 mm	W_1	0.8 mm
L_1	5 mm	W_2	0.2 mm
L_2	15.8 mm	W_3	0.7 mm
L_3	6 mm	W_4	0.3 mm
L_4	14 mm	θ	80^o
S	3.8 mm	d	3.1 mm

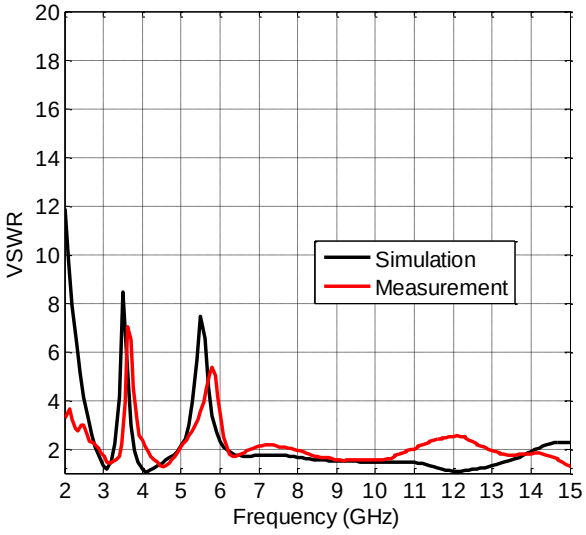

Figure 2. The simulated and measured VSWR of the proposed UWB antenna.

It can be observed that measurement agrees well with simulation, except in the range 11-13 GHz, which could be due to experimental tolerances, fabrication tolerances and the effect of the connector. The antenna works in the frequency band 2.9-15 GHz with the VSWR being less than 2, except around the notched frequencies. As desired, the antenna has filter characteristics around 3.5 GHz (the center frequency of WiMAX) and 5.5 GHz (the center frequency of WLAN). A small shift in the measured notched frequencies can be noticed, because the simulation environment is different from the real environment, as well as the fact that the substrate relative permittivity decreases as the frequency increases [17].

3. UWB MIMO ANTENNAS

In this section, utilizing the designed Pacman-shaped UWB antenna, two MIMO configurations are proposed. The first configuration is shown in Figure 3, in which the antenna elements are placed side by side a distance D from each other with separate ground planes and mounted on the same substrate. The two antenna elements are symmetric and have the same optimized parameters obtained for the single Pacman-shaped UWB antenna. The other configuration is

shown in Figure 4, in which the antenna elements are orthogonally placed on the same substrate and have separate ground planes. The centers of the circles are placed a vertical distance V and a horizontal distance h from each other, while having the same optimized parameters obtained for the single Pacman-shaped UWB antenna. After running several simulations and performing a parametric study, the optimum distances between the antenna elements are chosen as follows: D = 23 mm, h = 24 mm and V = 2 mm downward (i.e., the center of the right antenna is lower than the center of the left antenna).

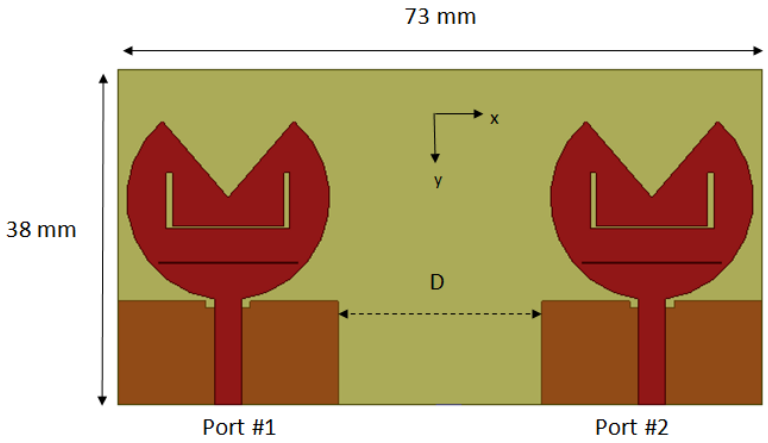

Figure 3. The structure of the proposed MIMO configuration #1.

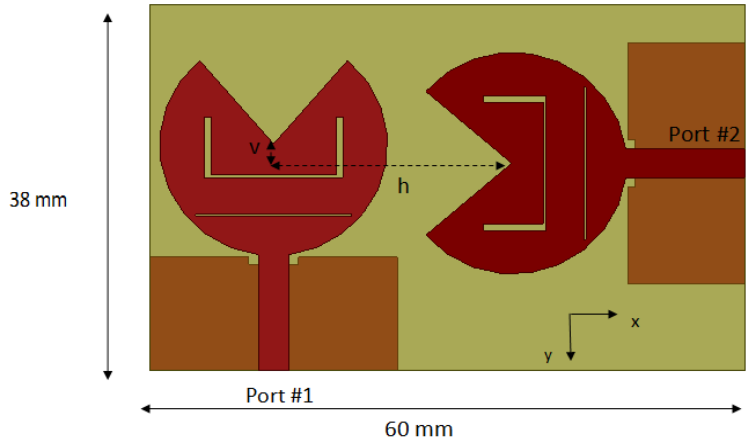

Figure 4. The structure of the proposed MIMO configuration #2.

The optimized distances were used to build the two configurations, then measurements were performed in the laboratory using Agilent VNA. Figure 5 shows a picture of the fabricated MIMO antennas.

Figure 6 illustrates the voltage standing wave ratio (VSWR) of the first MIMO configuration. It can be noticed that measurements agree well with simulation, except in the band 11-13 GHz, which could be due to the connectors and fabrication tolerance. Also, a shift in the notched frequencies occurs due to the reasons mentioned before. It is difficult to get a symmetric structure (i.e., $S_{22} = S_{11}$) in practice due to prototyping tolerances and connectors, which is clear from Figure 6 (i.e., the measured VSWR values of the two ports are somewhat different from each other). Figure 7 illustrates the VSWR of the second MIMO configuration.

Figure 5. Pictures of the fabricated MIMO configurations.

A good agreement exists between simulation and measurement when port 1 is excited, but a small difference between measurement and simulation appears in the band 11-15 GHz when port 2 is excited, which could be due to prototyping tolerances. Also, a shift in the notched frequencies appears as in the first configuration. It is clear that both antenna elements of the two configurations work in the UWB range.

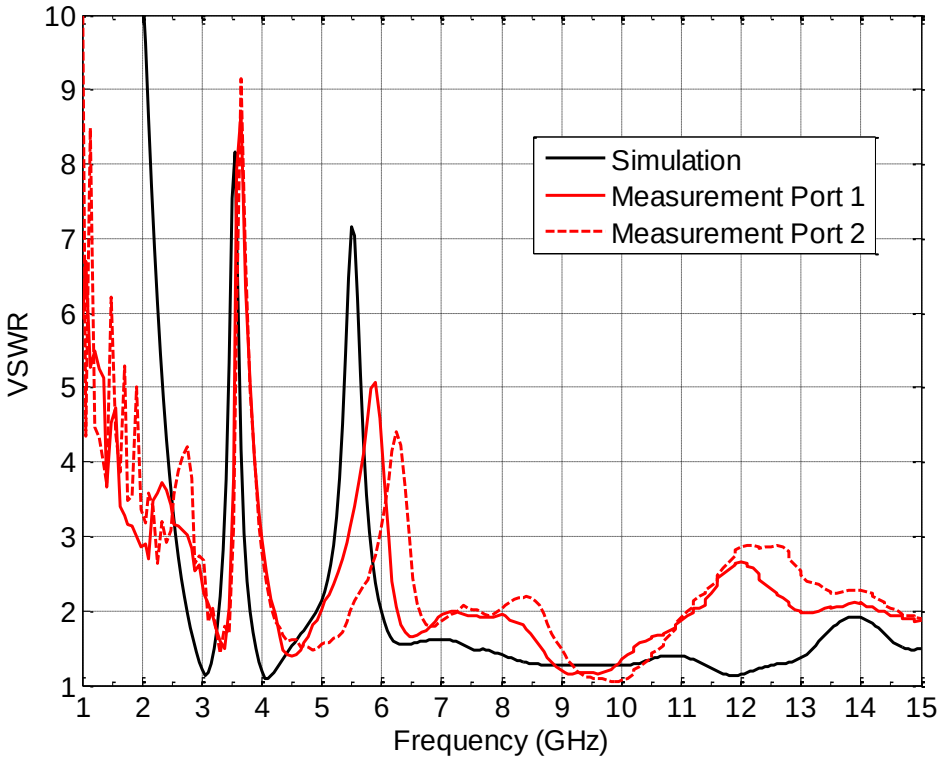

Figure 6. The simulated and measured VSWR of configuration #1.

One of the most important parameters while studying MIMO antennas is the isolation between the input ports. Figure 8 illustrates the isolation of the first and second MIMO configurations (i.e., S_{21} or S_{12}, since the networks are reciprocal ones). A good agreement exists between simulation and measurement with the isolation having measured values of more than 16 dB and 19 dB for the first and the second configuration, respectively. So, the orthogonal placement of the antenna elements achieves better isolation with smaller antenna size.

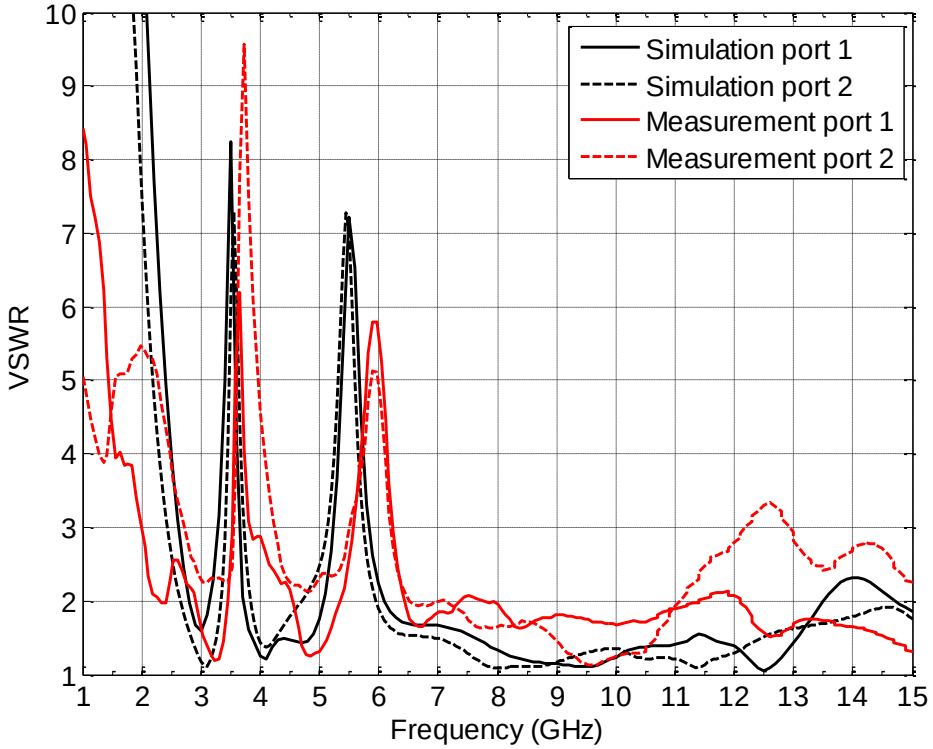

Figure 7. The simulated and measured VSWR of configuration #2.

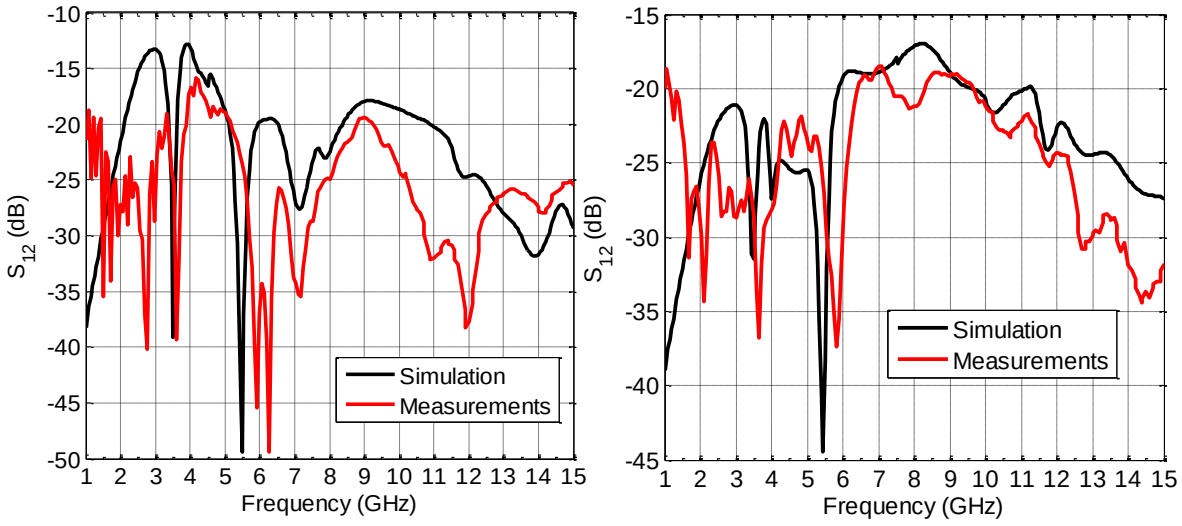

(a) (b)

Figure 8. S_{12} (in dB) of the proposed MIMO configurations.
(a) Configuration #1, (b) Configuration #2.

The E-plane and the H-plane patterns of the first configuration are illustrated in Figure 9. The radiation patterns of the first antenna element in Figure 9 (a) are obtained by exciting port 1 and terminating port 2 with a matched load. It is clear that the xz-plane is the H-plane and the yz-plane is the E-plane. As the frequency increases, the radiation pattern becomes distorted. The radiation patterns of the second antenna element in Figure 9 (b) are obtained by exciting the

second port and terminating the first port with a matched load. Due to symmetry, both antenna elements have the same radiation patterns, except that the H-plane of the second element has a 180^o shift. This is due to the way that the two antenna elements are placed beside each other. So, this configuration provides only spatial diversity.

The E-plane and the H-plane patterns of the second proposed UWB MIMO antenna are illustrated in Figure 10. The radiation patterns of the first antenna element in Figure 10 (a) are obtained by exciting port 1 and terminating port 2 with a matched load. It is difficult to obtain a pure omni-directional pattern, due to coupling between the antenna elements. It can be noticed that the xz-plane is the H-plane and the yz-plane is the E-plane. The radiation patterns of the second antenna element in Figure 10 (b) are obtained by exciting the second port and terminating the first port with a matched load. Here, the xz-plane is the E-plane and the yz-plane is the H-plane, which is the opposite of the first element, and this is due to the orthogonal placement of the antennas in the second configuration. Since the two elements have different patterns and opposite E-plane and H-plane, this configuration provides pattern and polarization diversity in addition to spatial diversity.

Now, the realized peak gain for each antenna element of both configurations is considered. In Figure 11 (a), the realized peak gain of the first element of configuration #1 is computed by exciting port 1 and terminating the other port with a matched load. The peak gain of the second element is almost the same due to symmetry. So, the result for port 1 is only shown. It can be noticed that the gain increases up to nearly 7 dBi in the whole band, but drops to nearly -8 dBi at the center frequency of WiMAX and to -3 dBi at the center frequency of the WLAN. In Figure 11 (b), the realized peak gain of both antennas in configuration #2 is computed by the same way. The gains of the two elements are slightly different due to asymmetry and they increase up to 7 dBi in the whole band, but drop to -5.5 dBi at the center frequency of WiMAX and to -3.8 dBi at the center frequency of the WLAN.

The current distribution is used to further study the operation of the UWB MIMO antennas. In Figure 12, the current distribution of the first configuration is obtained by exciting port 2 and terminating port 1 with a matched load. In Figure 13, the current distributions of both elements of the second configuration are computed by exciting the desired port and terminating the other with a matched load. It is clear from Figures 12 and 13, that the current is mainly concentrated at the edges of the circular patch and the feeding line of the excited element, except at 5.5 GHz, where the current is mainly concentrated at the WLAN notch and at 3.5 GHz, where the current is mainly concentrated at the U-shaped slot (WiMAX slot), and the current couples from port 1 to port 2 and *vice versa*.

Group delay has an important role in the dispersion characteristics of each antenna element. Due to symmetry in the first configuration, the simulated group delay of both elements is almost the same. So, only the result using S_{11} of the first antenna element is shown in Figure 14 (a), while in measurement one cannot guarantee symmetry; so, the group delay for both elements is shown in the same figure. In Figure 14 (b), the simulated and measured group delays of both elements of the second configuration are obtained using S_{11} and S_{22}. Both figures show almost a constant group delay, indicating that the dispersion is very small.

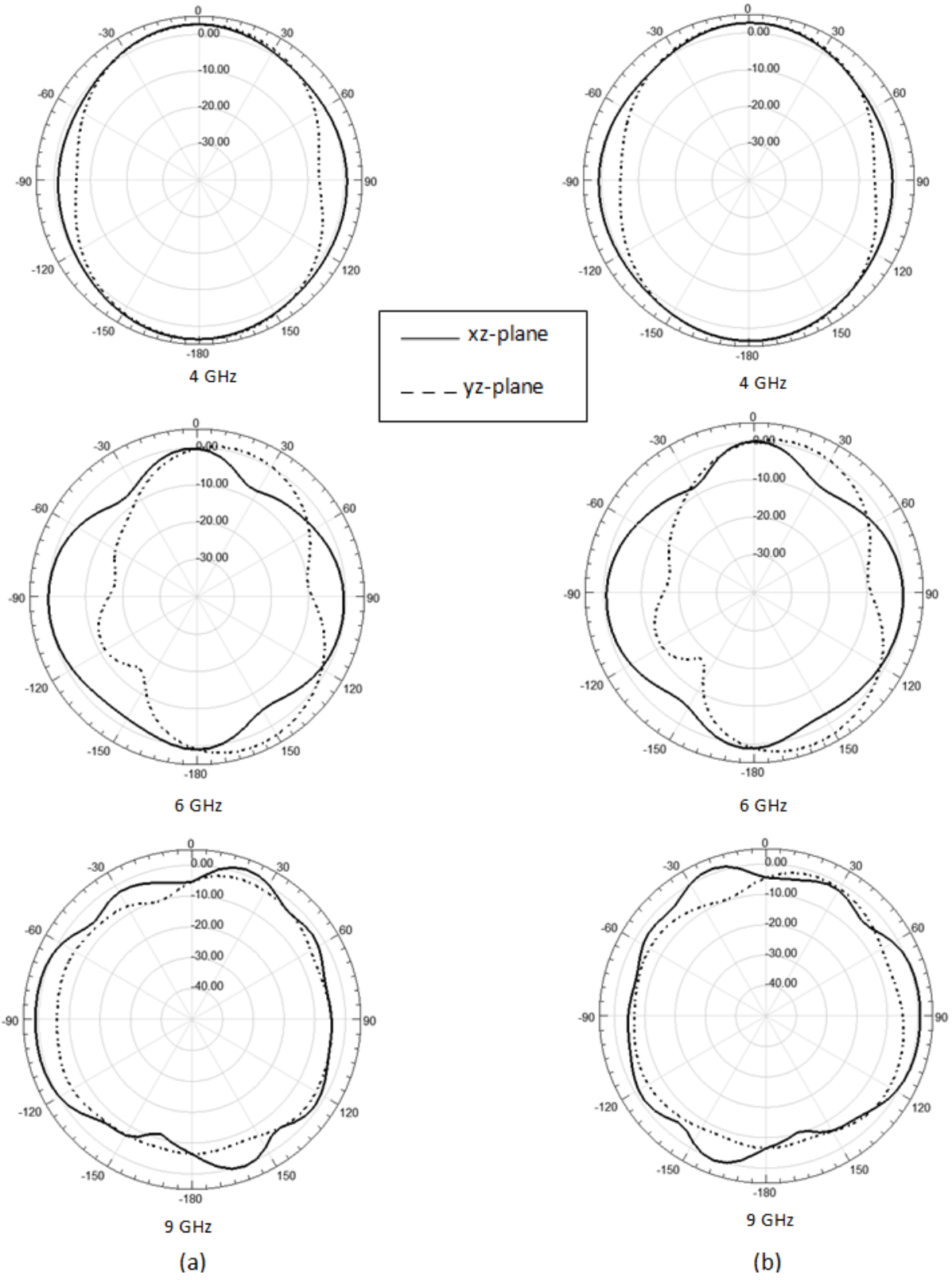

Figure 9. The simulated E-plane and H-plane radiation patterns (in dB) at 4, 6 and 9 GHz for the first MIMO configuration.
(a) Port 1 excited, (b) Port 2 excited.

Jordanian Journal of Computers and Information Technology (JJCIT), Vol. 2, No. 1, April 2016.

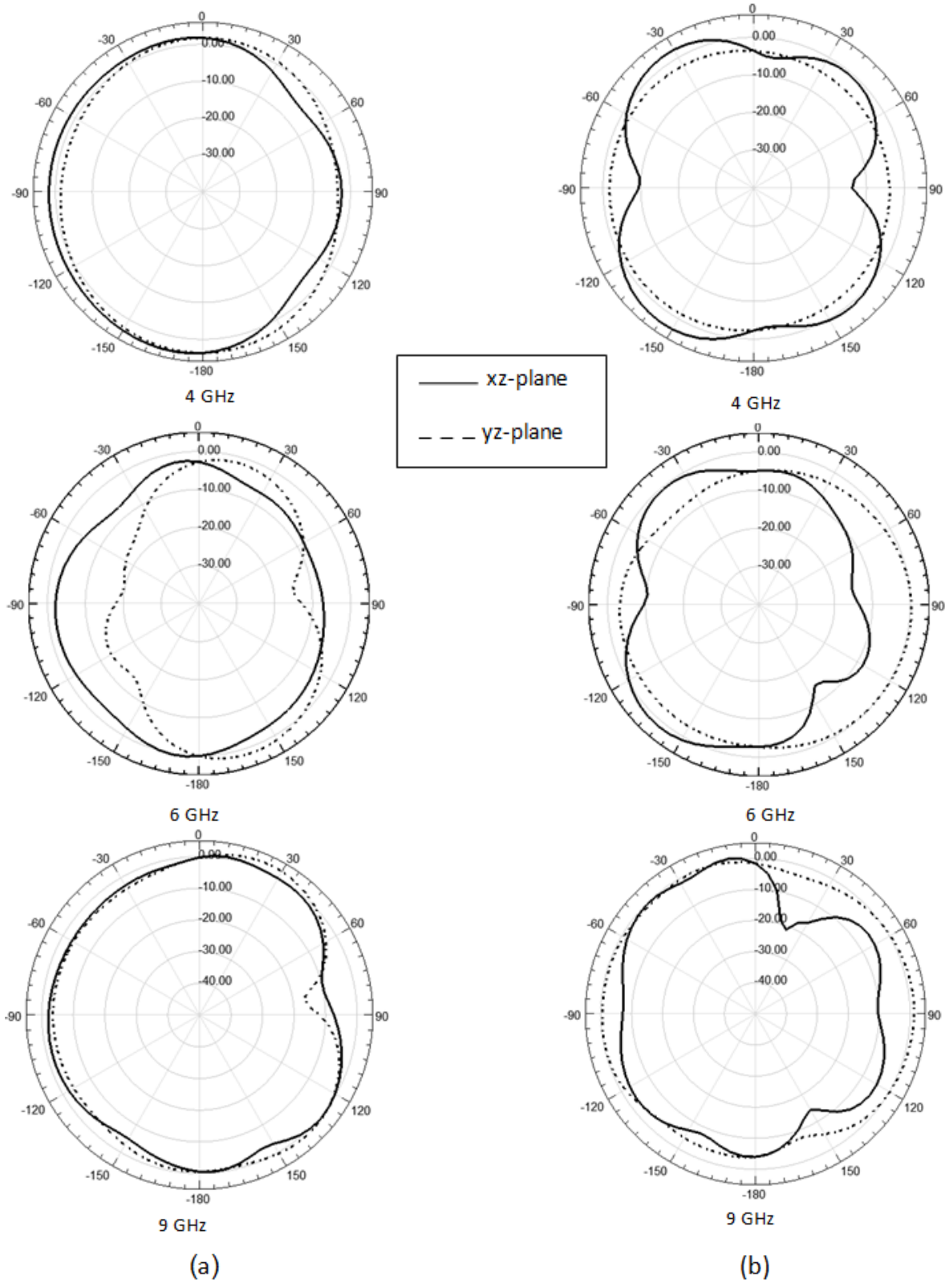

Figure 10. The simulated E-plane and H-plane radiation patterns (in dB) at 4, 6 and 9 GHz for the second MIMO configuration.
(a) Port 1 excited, (b) Port 2 excited.

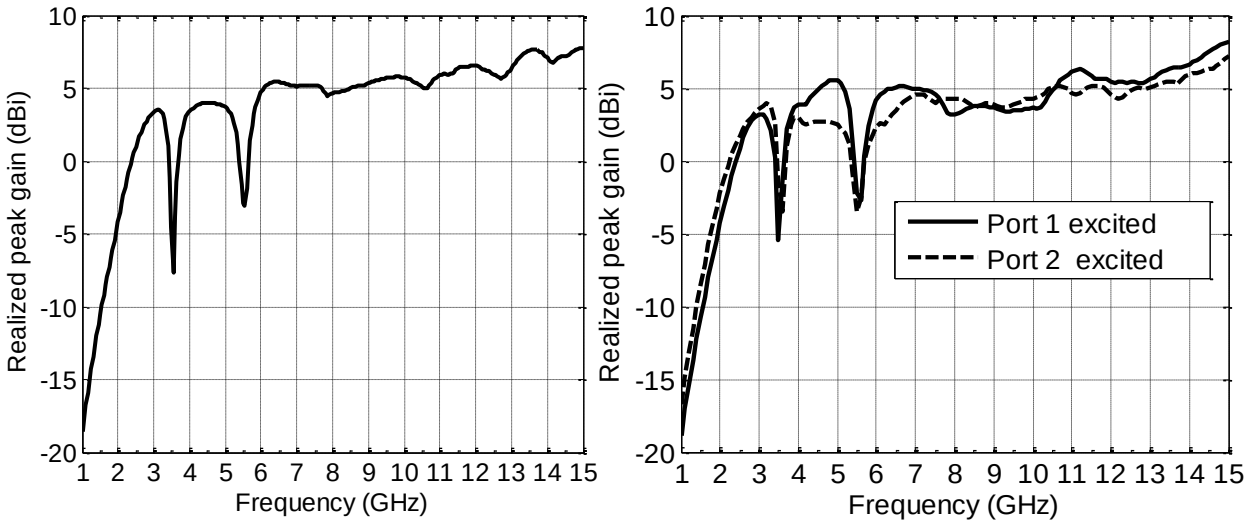

(a) (b)

Figure 11. The realized peak gain for both MIMO configurations.
(a) Configuration #1, (b) Configuration #2.

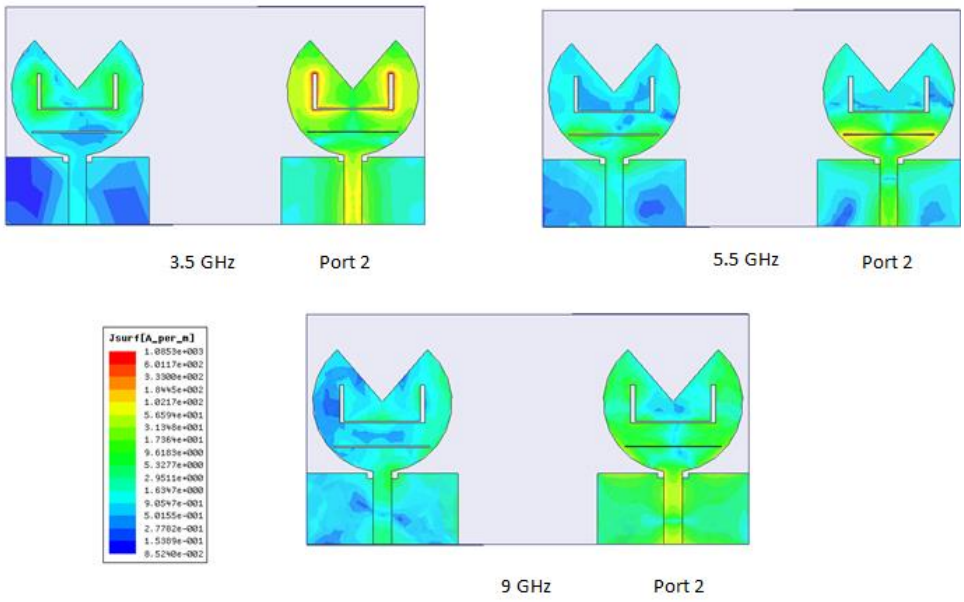

Figure 12. The current distribution of configuration #1 (port 2 excited) at 3.5, 5.5 and 9 GHz.

Jordanian Journal of Computers and Information Technology (JJCIT), Vol. 2, No. 1, April 2016.

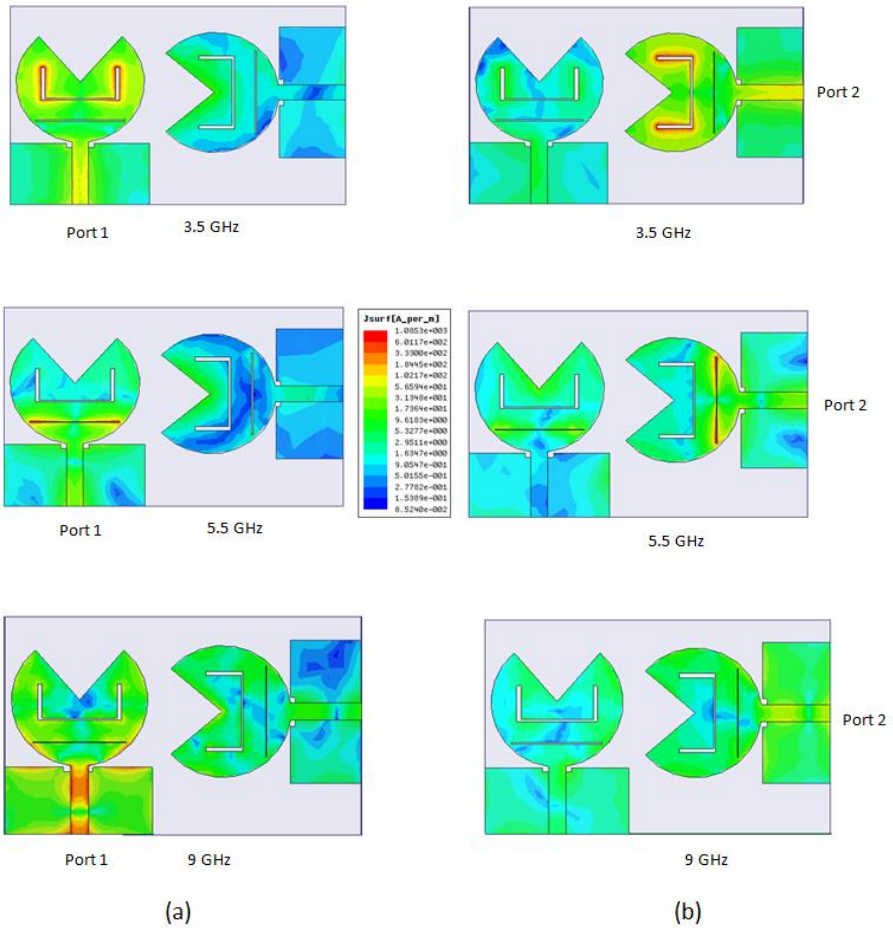

Figure 13. The current distribution of configuration #2 at 3.5, 5.5 and 9 GHz. (a) Port 1 excited, (b) Port 2 excited.

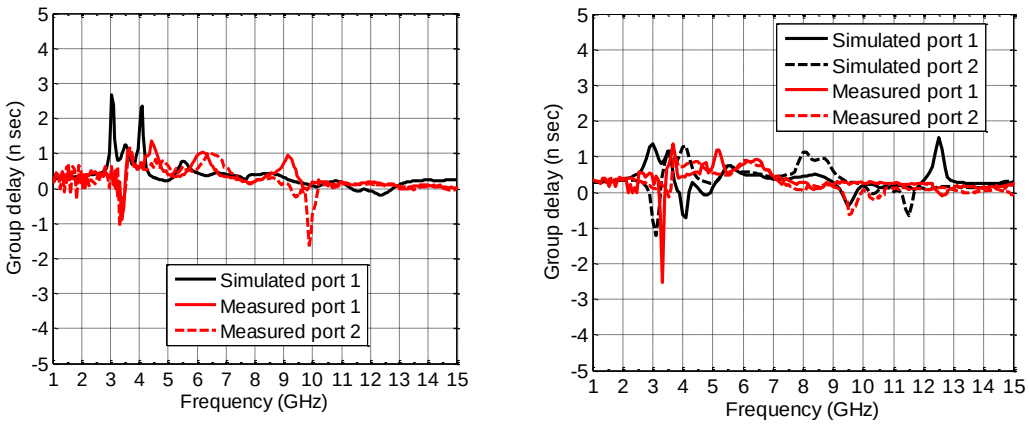

(a) (b)

Figure 14. Simulated and measured group delay for both MIMO configurations. (a) Configuration #1, (b) Configuration #2.

Another important parameter for MIMO antennas is the envelope correlation coefficient (ECC), which determines how much the communication channels are isolated. In other words, it describes how much the radiation patterns affect each other. For antennas having efficiency larger than 50%, the ECC can be computed from the scattering parameters [18]-[20]. The efficiency for both configurations is shown in Figure 15. Due to symmetry in the first configuration, the efficiency for both antenna elements is almost the same, so the results when port 1 is excited are shown in Figure 15 (a). In Figure 15 (b), the results for both antenna elements are shown. It is obvious that both configurations have efficiencies larger than 50% in the whole UWB range, except at the notched bands.

A value of 0.5 or less is adequate for low correlation between the antenna elements. The envelope correlation coefficients of the first and the second MIMO configurations were computed using the scattering parameters and are illustrated in Figure 16. The ECC of the first configuration in Figure 16 (a) is less than 0.05 in the whole band, which indicates a low correlation between the two elements' radiation patterns. So, the diversity gain will be high.

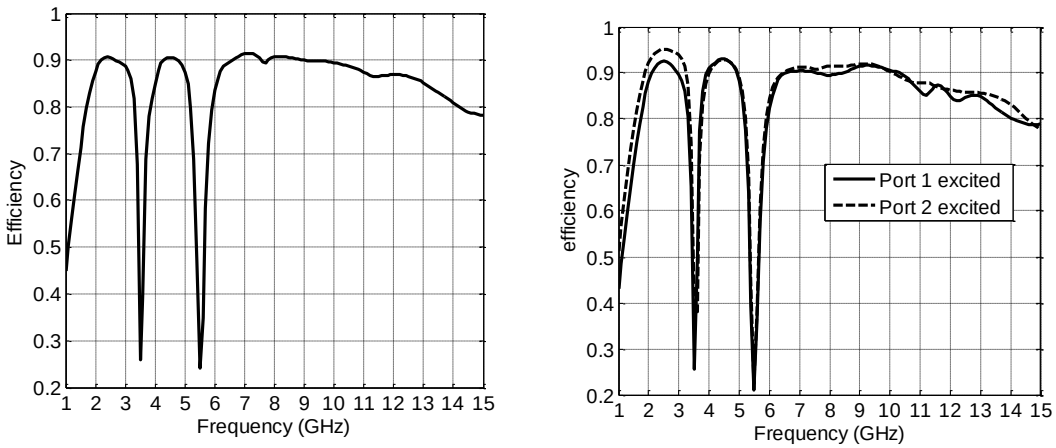

(a) (b)

Figure 15. The antenna efficiency for both MIMO configurations.
(a) Configuration #1, (b) Configuration #2.

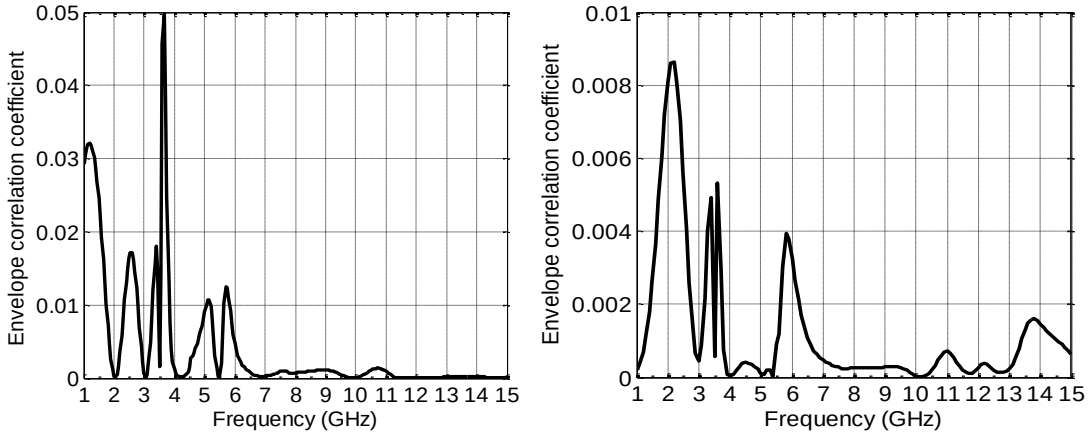

(a) (b)

Figure 16. The ECC for both MIMO configurations.
(a) Configuration #1, (b) Configuration #2.

Jordanian Journal of Computers and Information Technology (JJCIT), Vol. 2, No. 1, April 2016.

On the other hand, in Figure 16 (b), the second configuration has an ECC of less than 0.009 in the whole band, which indicates an even lower correlation between the two elements' radiation patterns. So, the diversity gain will be even higher. The ECC for the second configuration is smaller than that for the first one, and this is due to the orthogonal placement of the antennas.

Finally, the total active reflection coefficient (TARC) is considered. TARC is used to describe effectively the bandwidth and the efficiency of MIMO antennas. It accounts for coupling and random signal combinations between ports, as well as the effect of a feeding phase to the antenna port. For a desired port excitation, TARC is defined as the square root of the available power generated by all excitations minus radiated power, divided by the available power [18]-[21]. For lossless MIMO antenna, TARC can be computed from the scattering parameters of the antenna. The amplitude of all ports was kept at unity, while the excitation phases were varied with respect to port 1. For various phase differences between the ports' excitations, TARC curves were obtained to see the effect of the phase variation of the two ports on the antenna performance [22]. The TARC curves of the first and the second MIMO configurations are illustrated in Figure 17. It is clear that the bandwidth of the antenna and the notched frequency bands are slightly affected by the phase difference between the two input ports. A good property can be noticed, which is that the center frequency of the notched band is fixed when the phase difference is varied.

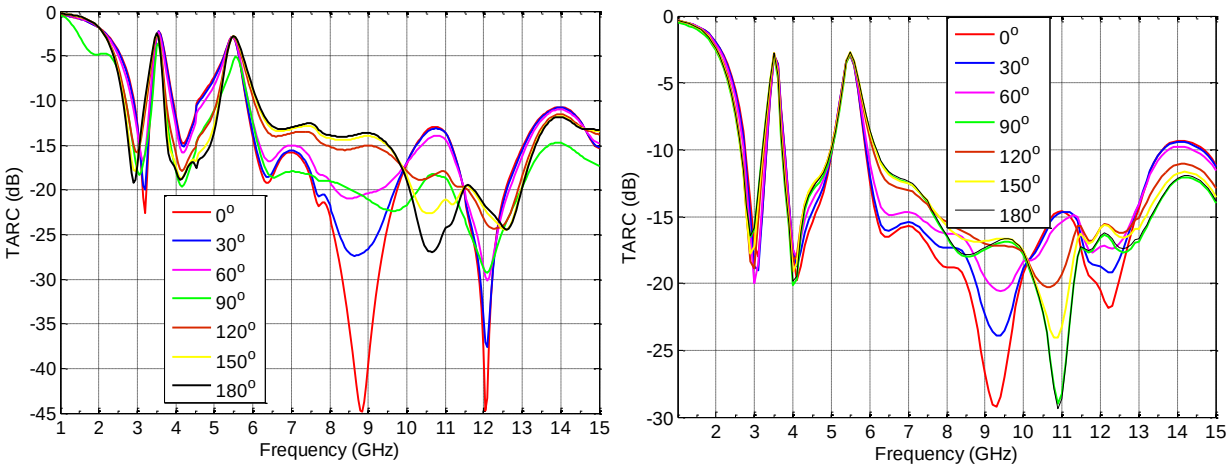

(a) (b)

Figure 17. TARC for both MIMO configurations.

(a) Configuration #1, (b) Configuration #2.

Table 2 lists a comparison between the proposed MIMO antennas and some other designs that have appeared in the literature. It is obvious that the proposed MIMO antennas have the largest bandwidth among the others with comparable isolation and ECC. In addition, the proposed antennas provide band rejection characteristics at the WLAN and WiMAX.

Table 2. Comparison between the proposed designs and previous designs.

Ref.	Size (mm^2)	Type	Bandwidth (GHz)	Isolation (dB)	ECC
[1]	27 × 47	Monopole	3.1 -10.6	> 17	< 0.01
[2]	40 × 68	Monopole	3.1 -10.6	> 15	< 0.01
[3]	40 × 40	Monopole	3.1-10.6	> 10	< 0.02
[4]	27 × 37	Monopole	2.35-10.82	> 18	< 0.05
[5]	38 × 91	Monopole	2.8-8	> 17	< 0.006
[6]	48 × 48	Slot	2.5-12	> 15	< 0.005
[7]	45 × 62	Monopole	3.1-10.6	> 20	-
[8]	40 × 40	Slot	3.1-10.6	> 18	< 0.005
[9]	26 × 40	Monopole	3.1-10.6	> 15	< 0.2
Configuration #1	38 × 73	Monopole	2.9-15	> 16	< 0.05
Configuration #2	38 × 60	Monopole	2.9-15	> 19	< 0.009

4. CONCLUSION

In this paper, the design and analysis of compact UWB MIMO antennas with two rejection bands were carried out. Two MIMO configurations were presented. In the first configuration, the two elements were placed beside each other, while in the second configuration, the two antenna elements were placed orthogonal to each other. Both elements work in the range 2.9-15 GHz with better than 10 dB return loss and an isolation of more than 16 dB and 19 for the first and the second MIMO configuration, respectively.

REFERENCES

[1] M. Khanl, M. F. Shafique, A. Capobianco, E. Autizi and I. Shoaib, "Compact UWB-MIMO Antenna Array with a Novel Decoupling Structure," IEEE, International Bhurban Conference on Applied Sciences and Technology (IBCAST), pp. 347-350, Islamabad, Pakistan, 15-19 Jan. 2013.

[2] A. Najam, Y. Duroc and S. Tedjni, "UWB-MIMO Antenna with Novel Stub Structure," Progress in Electromagnetics Research C, vol. 19, pp. 245-257, 2011.

[3] Ch. Mao and Q. Chu, "Compact Coradiator UWB-MIMO Antenna with Dual Polarization," IEEE Transactions on Antennas and Propagation, vol. 62, no. 9, pp. 4474-4480, September 2014.

[4] J. Zhao, Z. Zhang, Q. Liu, G. Fu and Sh. Gong, "Printed UWB MIMO Antenna with Different Polarizations and Band-Notch Characteristics," Progress in Electromagnetics Research Letters, vol. 46, pp. 113-118, 2014.

[5] M. Jusoh, M. Jamlos, M. Kamarudin and F. Malek, "A MIMO Antenna Design Challenges for UWB Applications," Progress in Electromagnetics Research B, vol. 36, pp. 357-371, 2012.

[6] P. Gao, Sh. He, X. Wei, Z. Xu, N. Wang and Y. Zheng, "Compact Printed UWB Diversity Slot Antenna with 5.5-GHz Band-Notched Characteristics," IEEE Antennas and Wireless Propagation Letters, vol. 13, pp. 367-379, 2014.

[7] Y. Cheng, W. Lu and Ch. Cheng, "Printed Diversity Antenna for Ultra-Wideband Applications," 2010 IEEE International Conference on Ultra-Wideband (ICUWB2010), vol. 1, pp. 1-4, 20-23 September 2010.

[8] J. Ren, D. Mi and Y. Yin, "Compact Ultra-Wideband MIMO Antenna with WLAN/UWB Bands Coverage," Progress in Electromagnetics Research C, vol. 50, pp. 121-129, 2014.

[9] L. Liu, S. Cheung and T. I. Yuk, "Compact MIMO Antenna for Portable Devices in UWB Applications," IEEE Transactions on Antennas and Propagation, vol. 61, no. 8, pp. 4257-4264, August 2013.

[10] J. Liang, Ch. Chiau, X. Chen and C.-G.Parini, "Study of a Printed Circular Disc Monopole Antenna for UWB Systems," IEEE Transactions on Antennas and Propagation, vol. 53, no. 11, pp. 3500-3504, November 2005.

[11] T. Wu, H. Bai, P. Li and X. Shi, "A Simple Planar Monopole UWB Slot Antenna with Dual Independently and Reconfigurable Band-Notched Characteristics," International Journal of RF and Microwave Computer-Aided Engineering, vol. 24, issue 6, pp. 706-712, November 2014.

[12] J. Ren and Y.-Z. Yin, "A Compact Dual Band-Notched Ultra Wideband Antenna with λ/4 Stub and Open Slots," Progress in Electromagnetics Research C, vol. 49, pp. 133-139, 2014.

[13] Y.-S. Li, X.-D. Yang, Q. Yang and C.-Y. Liu, "Compact Coplanar Waveguide Fed Ultra-Wideband Antenna with a Notch Band Characteristic," International Journal of Electronics and Communications, vol. 65, no. 11, pp. 961-966, 2011.

[14] J. Zang and X. Wang, "A Compact C-shaped Printed UWB Antenna with Band-Notched Characteristic," Progress in Electromagnetics Research Letters, vol. 43, pp. 15-23, 2013.

[15] M. Ojaroudi, G. Ghanbari, N. Ojaroudi and C. Ghobadi, "Small Square Monopole Antenna for UWB Applications with Variable Frequency Band-Notch Function," IEEE Antennas and Wireless Propagation Letters, vol. 8, pp. 1061-1064, 2009.

[16] ANSYS-High Frequency Structure Simulator (HFSS), Ansys, Inc., Canonsburg, Pennsylvania, USA, 2011.

[17] S. Mumby and J. Yuan, "Dielectric Properties of FR-4 Laminates as a Function of Thickness and the Electrical Frequency of the Measurement," Journal of Electronic Materials, vol. 18, issue 2, pp. 287-292, March 1989.

[18] M. S. Sharawi, "Printed Multi-Band MIMO Antenna Systems and Their Performance Metrics," IEEE Antennas and Propagation Magazine, vol. 55, no. 5, pp. 218-232, October 2013.

[19] M. S. Sharawi, "Printed MIMO Antenna Systems: Performance Metrics, Implementations and Challenges", (invited paper), Forum in Electromagnetic Research Methods and Application Technologies (FERMAT), ART-2014-01-010, pp. 1-11, February 2014.

[20] M. S. Sharawi, Printed MIMO Antenna Engineering, Artech House, ISBN: 978-1-60807-681-9, 2014.

[21] M. Manteghi and Y. Rahmat-Samii, "Broadband Characterization of the Total Active Reflection Coefficient of Multiport Antennas," IEEE Antennas and Propagation Society International Symposium, vol. 3, pp. 20-23, 22-27 June 2003.

[22] M. Sharawi, "A 5-GHz 4/8-Elements MIMO Antenna System for IEEE 802.11AC Devices," Microwave and Optical Technology Letters, vol. 55, no. 7, pp. 1589-1594, July 2013.

ملخص البحث:

في هذا البحث، يتمّ تصميم هوائي أحادي القطب ذي نطاق فائق العرض وتحليله وبناء نموذج أولي له. والهوائي موضوع البحث هوائي مدمج ذو قطاع جانبي منخفض، مع ثلميْن في نطاقه الترددي. بعدئذ، يجري استخدام الهوائي في شكلين متعدّدي المداخل والمخارج. ويتم تركيب الهوائيان على طبقة أساس منخفضة التكاليف ذات ثابت عزل يساوي 4.4. الشكل الأصلي لعنصر الهوائي المنفرد دائري بنصف قطر مقداره 11.5 مم، ثم أُزيل قطاع من التوصيلة المؤقتة (مما يجعله هوائياً على شكل باكمان)؛ من أجل تحسين عرض نطاق الممانعة. وتوفر الهوائيات المقترحة عرض نطاق ممانعة يتراوح من 2.9 إلى 15 غيغاهيرتز، بفقد إرجاع أفضل من 10 ديسيبل، وعزل أكثر من 16 ديسيبل و19 ديسيبل للشكلين متعدّدي المداخل والمخارج الأول و الثاني، على الترتيب.

علاوة على ذلك، يمكن للهوائيات أن تنبذ التداخلات الناجمة عن إمكانية التشغيل المتبادل لمنفذ الميكروويف على مستوى العالم (واي ماكس) بتردد مركزي مقداره 3.5 غيغاهيرتز، وشبكة المنطقة المحلية اللاسلكية بتردد مركزي مقداره 5.5 غيغاهيرتز.